Available online at www.sciencedirect.com
SCIENCE DIRECT
International Journal of Mass Spectrometry 248 (2006) 87–102
International Journal of Mass Spectrometry
www.elsevier.com/locate/ijms

Review

Microplasmas, an emerging field of low-temperature plasma science and technology

R. Foest [a], M. Schmidt [a], K. Becker [b,c,*]

[a] *Institut für Niedertemperaturplasmaphysik (INP), Friedrich-Ludwig Jahn Strasse 19, D-17489 Greifswald, Germany*
[b] *Department of Physics and Engineering Physics, Stevens Institute of Technology, Hoboken, NJ 07030, USA*
[c] *Center for Environmental Systems, Stevens Institute of Technology, Hoboken, NJ 07030, USA*

Received 15 October 2005; received in revised form 14 November 2005; accepted 15 November 2005
Available online 28 December 2005

Abstract

Spatially confining atmospheric pressure, non-equilibrium plasmas to dimensions of 1 mm or less is a promising approach to the generation and maintenance of stable glow discharges at atmospheric pressure. Such microdischarges or microplasmas represent systems with new and fascinating challenges for plasma science such as the possible breakdown of "*pd* scaling" and the increasing dominance of boundary-dominated phenomena. Pulsed excitation on a sub-microsecond time scale results in microplasmas with significant shifts in both the temperatures and energy distribution functions of ions and electrons. This allows for the selective production of chemically reactive species and opens the door to a wide range of new applications of microplasmas in areas such as environmental remediation, biology and biomedicine, intense light sources in the ultraviolet and vacuum ultraviolet, and gas and surface analysis — to name just a few. This topical review addresses some of the scientific challenges and technological opportunities afforded by microplasmas.

Keywords: Plasma; Gas discharge; Microplasma; Weakly ionized gas; Hollow cathode

Contents

* Corresponding author. Tel.: +1 201 216 5671; fax: +1 201 216 5638.
E-mail address: kbecker@stevens.edu (K. Becker).

1387-3806/$ – see front matter © 2005 Elsevier B.V. All rights reserved.
doi:10.1016/j.ijms.2005.11.010

1. Introduction and background

The plasma state is often referred to as the 4th state of matter. A plasma is characterized by the presence of positive (and sometimes also negative) ions and negatively charged electrons in a neutral background gas. Most of the matter in the universe is in the plasma state. Examples include the sun and other stars, interstellar matter, cometary and planetary atmospheres, and the terrestrial ionosphere. Naturally occurring plasmas on earth are rare and include lightning and flames. Plasmas are generated primarily for technological applications, which include welding arcs, plasma torches, high pressure and fluorescent lamps, the ignition spark in an internal combustion engine, and the vast range of low-pressure plasmas employed in the fabrication of microelectronic devices. Magnetically confined plasmas in nuclear fusion reactors are one of several choices to achieve the extreme conditions, under which controlled nuclear fusion might occur in the laboratory. Plasmas are created by supplying energy to a volume containing a neutral gas, so that a certain fraction of free electrons and ions are generated from the neutral constituents. In technical plasma devices, the plasma is generally generated in electrical discharges and the input energy is supplied in the form of electrical energy.

Plasmas can be categorized as either “thermal (or ‘hot’) plasmas” or “non-thermal (or ‘cold’) plasmas.” The main constituents (ions, electrons, neutrals) of a thermal plasma are in thermodynamic equilibrium and can be characterized by a single temperature. This temperature can vary from a few thousand Kelvin for a plasma torch to more than a million Kelvin in fusion plasma devices and in the interior of stars. In a non-thermal plasma, the electron temperature is much higher (10,000 K to more than 100,000 K) than the temperature of the ions and neutrals, which are roughly the same and range from room temperature (300 K) to about 2500 K. We note that the concept of a thermodynamic temperature requires that the energy distribution of the particles in question can be described by a Maxwell–Boltzmann distribution function corresponding to a single temperature. This is usually not the case for the electrons in a non-thermal plasma, whose energy distribution function is typically highly non-Maxwellian. Nevertheless, the nomenclature “electron temperature” is also commonly used in these cases. Because of the fact that electrical discharges are the most widely used way to generate low-temperature, non-equilibrium plasmas, the low-temperature plasma community often uses the terms “discharge” and “plasma” interchangeably. In this article, we use the term “plasma” to denote a plasma that is generated by an electrical discharge.

Faraday was the first to realize that an ionized gas has unique properties and he documented his observations in three books published in the mid 19th century [1–3]. Many experiments were carried out at reduced pressure, which had the advantage that only moderate voltages were required to start the discharge and that the entire discharge vessel could be filled with plasma. Progress in gas discharge physics depended heavily on the development of vacuum technology and the availability of adequate voltage sources. Faraday introduced the concept of ions as carriers of electricity and distinguished between cathode and anode and he even distinguished between cations (moving to the cathode) and anions (passing to the anode). The term plasma was coined much later by Langmuir and Tonks [4]. The work of Wilson [5] and Townsend and Hurst [6,7] in the early 20th century established that conductivity in discharges was due to ionization of atoms or molecules by electron collisions. It was obvious early on that cold glow discharge plasmas had properties that were very different from those of hot arc discharges. For a long time it was believed that non-thermal plasmas could exist only at low pressure and were the only plasmas that could be generated in large volumes. We now know that non-thermal plasmas can also be generated at high pressure (incl. atmospheric pressure), albeit not easily in large volumes. The properties of non-equilibrium plasmas are discussed in many books and publications (see e.g., [8–10] and references therein), to which we refer the interested reader for further details.

High-pressure plasmas represent an environment where collisions and radiative processes are dominated by (i) step-wise processes, i.e., the excitation of excited states followed by collisions of the excited species with other particles resulting in new energy transfer routes and by (ii) three-body collisions leading, e.g., to the formation of excimers. The dominance of collisional and radiative processes beyond binary collisions involving ground-state species allows for many applications of high-pressure plasmas such as high power lasers, opening switches, novel plasma processing applications and sputtering, electromagnetic absorbers and reflectors, remediation of gaseous pollutants, medical sterilization and biological decontamination, and excimer lamps and other non-coherent vacuum ultraviolet (VUV) light sources [11]. However, self-sustained diffuse plasmas tend to be unstable at high pressure due to their susceptibility to filamentation and the transition to an arc (see [8–10,12]), which limits their practical utility. A promising approach to generate and maintain stable high-pressure plasmas is based on the recognition that plasmas confined to critical dimensions below about 1 mm, so-called “microplasmas,” display a remarkable stability towards arcing. There are several factors that contribute to the stabilization of microplasmas, not all of them fully understood at this point in time. One stabilizing factor can be explained in terms “*pd* scaling.” The voltage required to ignite a discharge, the so-called breakdown voltage, depends on the product of pressure “*p*” and electrode separation “*d*” as shown schematically in Fig. 1 (Paschen curve). If one increases the pressure for a

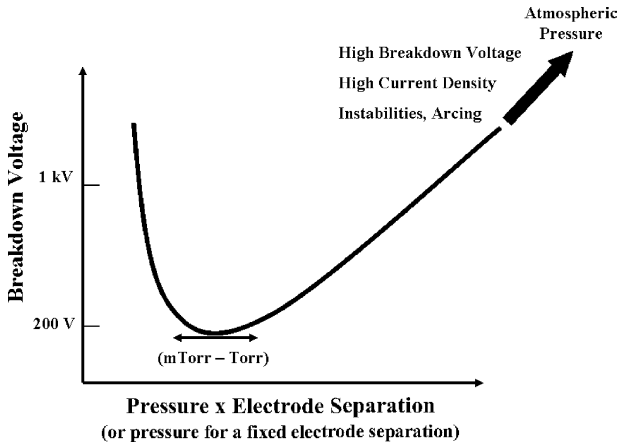

Fig. 1. Schematic diagram of a Paschen curve, i.e., a plot of the breakdown voltage vs. the product of pressure and electrode separation.

fixed value of "*d*," the required breakdown voltage increases. At atmospheric pressure (and electrode separations of centimeters to tens of centimeters, which are typical for low-pressure plasmas), breakdown voltages in the kV range are required to ignite the discharge. The high breakdown voltage leads to a high current density after the discharge is ignited, particularly in the cathode fall of the discharge. The high current density is the source of discharge instabilities in the cathode fall region, which quickly lead to the formation of an undesirable arc. As a consequence of "*pd* scaling," the breakdown voltage can be kept low, if the electrode separation "*d*" is reduced when the pressure "*p*" is increased. At atmospheric pressure, *d*-value below 1 mm are required to be near the minimum in the Paschen curve for essentially all gases. Another factor that at least in part contributes to the stability of high-pressure microplasmas are the high losses of charge carriers to the surrounding walls. The typical operating parameters of microplasmas (pressures up to and exceeding 1 atm (760 Torr) and dimensions below 1 mm) correspond to "*pd*" values of between 1 and 10 Torr cm. These "*pd*" values are similar to those for large volume, low-pressure plasmas. However, the current and the energy densities in microplasmas are much higher. This results in an effective gas heating and momentum transfer from the electrons to the gas molecules and causes gas dynamics [13].

We note that the terminology "microdischarge" has been used in the gaseous electronics community in a much narrower sense referring to the filament in a dielectric barrier discharge (DBD). Here, we use the term in a broader sense for electrical discharges ignited in small spatial volumes, i.e., a microdischarge is a miniaturized (high-pressure) discharge. The filamentary discharge in a DBD is a topic that has been discussed extensively in the literature [14] and will not be discussed here. Also, the well-developed field of flat panel plasma displays, which use thousands of individual microdischarges is not a topic of this review. On another matter of nomenclature, one can distinguish between unbounded microdischarges such as a filament in a DBD or a corona discharge near a sharp tip electrode and bounded microdischarges, where the size of the discharge is determined by the dimensions of the spatial cavity in which the discharge is generated.

In this topical review, we discuss some basic properties of high-pressure microplasmas generated in a variety of geometries using a wide range of excitation modes and discuss selected microplasma applications. We will limit the discussion of microplasma applications to areas that are of particular interest to the audience of this journal.

2. History of microdischarges

2.1. The microhollow cathode discharge (MHCD)

Microdischarges generated in spatially confined cavities began to appear in the literature in the mid-1990s. Schoenbach et al. [15] were the first to report the stable atmospheric pressure operation of a microdischarge in a cylindrical hollow cathode geometry (Fig. 2a). These authors coined the term "microhollow cathode discharge (MHCD)" for this type of microdischarge, which was subsequently used by several other groups [16–21]. The phrase "hollow cathode" historically refers to a specific mode of discharge operation, in which the sustaining voltage drops as the current increases, i.e., the discharge has a "negative differential resistance" (hollow cathode or negative glow mode). Nowadays, MHCDs are often not operated in the hollow cathode mode, but as normal or abnormal glow discharges.

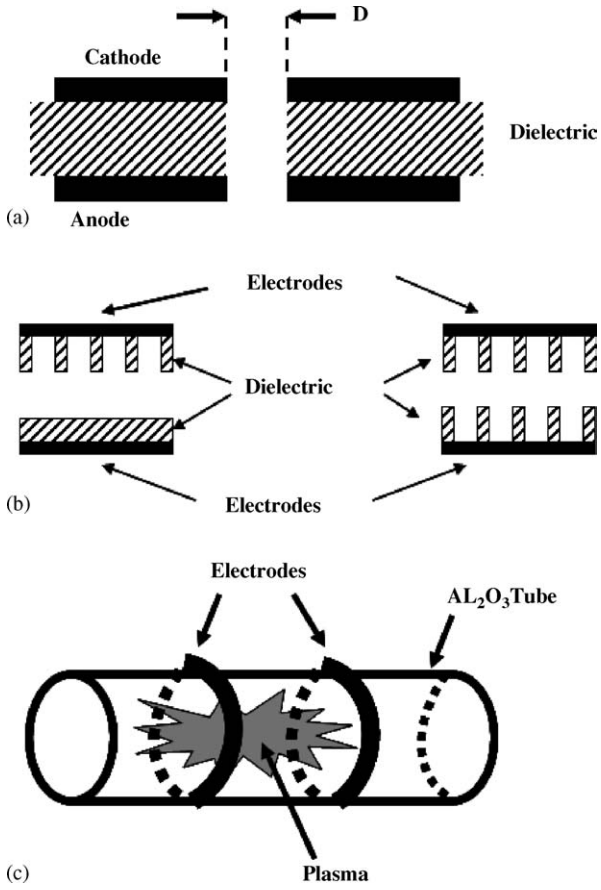

Fig. 2. Schematic diagrams of (a) a microhollow cathode discharge (MHCD) configuration, (b) a capillary plasma electrode (CPE) discharge configuration, and (c) a cylindrical dielectric barrier discharge (C-DBD) configuration.

Therefore, the inclusion of the phrase 'hollow cathode' in the name MHCD might be misleading. As a consequence, other groups have been referring to these discharges to simply as "microdischarges" [22,23] or "microstructured electrode arrays" [24]. Another indication that MHCDs are not merely an extension of the low-pressure hollow cathode (HC) discharge to higher pressures is the fact that their observed stable operation at cathode openings of 250 μm at atmospheric pressure (in air) violates the "White-Allis" similarity law [25,26], which relates the discharge sustaining voltage V of a HC discharge to the product (pD) and the ratio (J/p), where J is the discharge current density, p is the pressure, and D is the diameter of the opening in the cathode. Thus, high-pressure operation of a HC discharge can be accomplished by reducing the size D of the hole in the cathode (Fig. 2a). Based on the empirically established upper limit of around 10 Torr· cm in the rare gases [27], atmospheric pressure operation would require hole sizes of about 10 μm (assuming that the gas is at room temperature). This is a factor of 25 less than what was observed empirically. This indicates that physical processes other than pendulum–electron coupling between "opposite" cathodes must be present to account for the negative differential resistance and the discharge stability at high pD values. In light of the above, and in an effort to avoid confusion, i.e., blurring the distinction between discharge device geometry or structure and its operational characteristics, we will no longer use the phrase "microhollow cathode discharge, MHCD" and adopt the general terms "microplasma," "microcavity plasma," or "microdischarge" [28].

Frequently, applications of microdischarges require the use of two-dimensional arrays of individual microdischarges, either operated in parallel or in series, or both. Microdischarges can be operated in parallel without individual ballast resistors, if the discharges are operated in the range where current–voltage (I–V) curve has a positive slope [15,20,24,29,30]. In regions where the I–V characteristics has a negative slope (hollow cathode mode) or is flat (normal glow mode), arrays can be generated by using a distributed resistive ballast such as semi-insulating silicon as anode material [31] or multilayer ceramic structures where each microdischarge is individually ballasted [32,33].

2.2. The capillary plasma electrode discharge

The operating principles of the capillary plasma electrode (CPE) discharge are much less well understood than those of many other microdischarges. The CPE discharge uses a novel electrode design introduced by Kunhardt and Becker [34], which employs dielectric capillaries that cover one or both electrodes of a discharge device (Fig. 2b). In many other aspects the CPE discharge looks similar to a conventional dielectric barrier discharge (DBD). However, the CPE discharge exhibits a mode of operation that is not observed in DBDs, the so-called "capillary jet mode." The capillaries, with diameters in the range from 0.01 to 1 mm and length-to-diameter (L/D) ratios from 10:1 to 1:1, serve as plasma sources and produce jets of high-intensity plasma at high pressure, which emerge from the end of the capillary and form a "plasma electrode." The CPE discharge displays two distinct modes of operation when excited by pulsed dc or ac. When the frequency of the applied voltage pulse is increased above a few KHz, one observes first a diffuse mode similar to the diffuse glow described of a DBD as described by Okazaki et al. [35]. When the frequency reaches a critical value (which depends strongly on the L/D value and the feed gas), the capillaries "turn on" and bright, intense plasma jets emerge from the capillaries. When many capillaries are placed in close proximity to each other, the emerging plasma jets overlap and the discharge appears uniform. This "capillary" mode is the preferred mode of operation of the CPE discharge and has been characterized for several laboratory-scale research discharge devices in terms of its electrical and plasma properties [36–41].

2.3. Microplasmas for chemical analysis

Shortly after the introduction of the MHCD in 1996 [15] and the CPE discharge in 1997 [37,38], a variety of microplasma sources were developed for chemical analysis purposes. Rapid advances in microfabrication techniques facilitated the miniaturization of known plasma concepts and their integration into "lab-on-a chip" analytical tools such as plasma atomic spectrometry, plasma mass spectrometry, and plasma gas and liquid chromatography. Miniature inductively and capacitively coupled plasmas, often generated in capillary tubes, are among the most widely used plasma sources used for chemical analysis. Other concepts such as microwave plasmas, microdischarges in hollow cathode geometries and microstructure electrode (MSE) discharges have been utilized in the past few years [42]. The main driving forces behind the miniaturization of bench-scale chemical analysis tools include:

- the desire to improve the cost-to-performance ratio of analytical procedures in terms labor invested and low cost of instrument, instrument operation, and instrument maintenance, while maintaining acceptable detection limits and without compromising the reliability of the results;
- it may enable faster analysis as a result of reduced transport length;
- the ability to utilize very small amounts of samples and reagents;
- the potential for portability (small apparatus including small power supply) which will make possible the use of the instrument in the field or on the spot (in situ analysis).

Several pioneering papers describing the use of microplasmas in chemical analysis applications appeared in the last 1990s. Brede et al. coupled a microplasma mass spectrometer to a gas chromatograph for element-selective detection of halogen atoms [43]. Broekaert and co-workers introduced a microplasma excitation and ionization source for atomic emission spectrometry of gaseous species and Hg [44,45]. Hopwood and coworkers developed portable gas analyzers by coupling microfabricated inductively coupled plasma sources with miniaturized Fabry-Perot interferometers [46]. Two recent review articles by Broekaert [47] and Karanassios [42] provide a summary of recent developments in the use of microplasma sources in instruments for respectively, spectrochemical and chemical analyses.

2.4. Other microdischarges

In addition to the original MHCD concept, other geometries based on the hollow cathode design have been used such as parallel plates, holes of any shape in a solid cathode, slits in the cathode, spirals [48], micro-tubes with the anode at the orifice [49], or inserted through the walls [21], and micro-slots [50]. Common to all these geometries are the dimensions of the cathode hollows, which are on the order of 100 μm.

Another type of microdischarge, whose characteristic plasma dimensions are near the upper end of the 1 mm size scale that we use to define microdischarges, is a variant of the DBD, the so-called cylindrical dielectric barrier discharge (C-DBD), which was first introduced by Laroussi [51] and has been used extensively by Masoud et al. [52–54] (Fig. 2c). This discharge source consists of a dielectric tube (alumina, Al_2O_3) with an outer diameter of about 6 mm and an inner diameter around 3 mm. Two straps of Cu are wrapped around it, separated by a fixed distance (2.5 mm), which serve as the two electrodes. A 13.56 MHz rf power generator, capable of delivering up to about 100 W, is applied to the two electrodes. The power source generates and sustains a stable discharge plasma inside the tube that is limited to the space between the electrodes, but typically has a diameter of less than 2 mm. In order to maximize the power that the rf generator delivers into the plasma, a matching network is used to match the impedance of the load (the plasma) with the output impedance of the generator. Alternatively, the C-DBD can also be excited by mid-frequency ac power (100–400 kHz).

Jet plasmas are another variant of the above source. A jet discharge is ignited in a quartz capillary (of about 1 mm inner diameter) by coupling power capacitively to two ring electrodes on the outside of the capillary at 27 MHz [55]. The working gas flows through the capillary and forms a jet. The use of molecular gases such as nitrogen or air requires another geometry in which a rod inside a capillary of an inner diameter of about 2.5 mm serves as one of the electrodes. Both sources can be operated at powers between 5 and 25 W and carrier gas flows between 3 and 10 slm per capillary. The construction of capillary arrays has also been achieved and has been tested successfully for surface modification applications.

3. Diagnostics of microplasma and microplasma properties

Extensive diagnostics studies of various microplasmas have been carried out using a variety of established techniques ranging from electrical characterization to various optical diagnostics methods and plasma mass spectrometry. These include time-averaged as well as time-resolved studies. As a result, there is a fairly broad data base on the basic parameters that characterize microplasmas incl. *I–V* characteristics, electron density and temperature as well as electron energy distribution, gas temperature, radiative properties, etc. Because of the small spatial extent of most microplasmas, the vast majority of these studies yielded results averaged over the size of the microplasma. Recently, there have been two notable examples of spatially resolved microplasma diagnostics studies. Wagner and co-workers [56] reported the result of spatially and temporally resolved optical diagnostics studies of an isolated filamentary discharge in a DBD using cross correlation spectroscopy. Donnelly and co-workers [57] used optical emission spectroscopy with a 6 μm spatial resolution to determine the gas temperature profile across a 200 μm wide atmospheric pressure He microplasma. Clearly, further time- and space-resolved diagnostics studies will be needed to gain insight into the intricate properties of microplasmas.

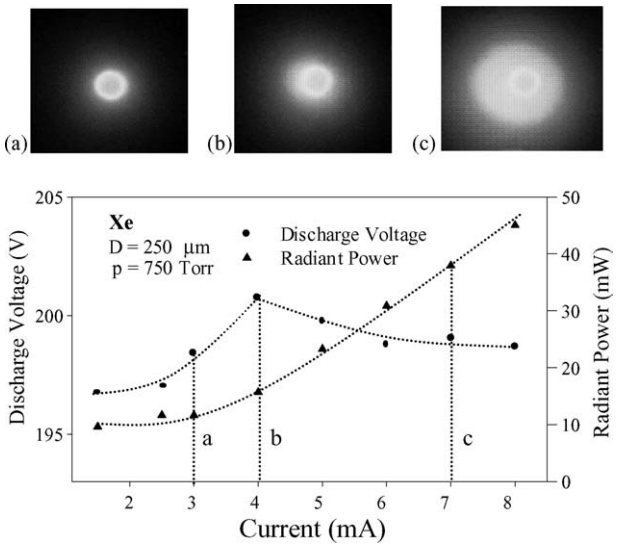

Fig. 3. (a) (upper part): end-on photographs of microdischarges in Xe at a pressure of 750 Torr for various currents. The photographs were taken through an optical filter, which allowed only the excimer radiation to pass; (b) (lower part): *I–V* characteristic of the microdischarge and VUV radiant power as a function of current.

3.1. Modes of microplasma operation

Microplasmas in various configurations can be excited by direct current (dc), pulsed dc, alternating current (ac), and radio frequency (rf) and microwave sources. The dc *I–V* curve of microdischarges shows distinct regions. Fig. 3 shows the *I–V* curve for a discharge in Xe at 750 Torr together with images of the discharge obtained in the UV at a wavelength of 172 nm [29]. The plasma is confined to the hole as long as the current is very low. It expands beyond the microhole when the discharge mode changes to a normal glow discharge. If the cathode surface is limited, the discharge enters an abnormal glow.

Pulsed excitation of microdischarges reduces the thermal load on the electrodes at higher currents. Pulse widths from ms to ns at various duty cycles have been used. Pulsed excitation with sub-μs pulse widths causes significant changes in the plasma parameters and a noticeable increase in the excimer emission intensity as observed in Ar and Xe microdischarges, which is attributed to pulsed electron heating [58]. The electron temperature is increased during the short pulse, but the change in the gas temperature is insignificant. The shift in the electron energy distribution function to higher energy leads to an increase in the ionization and excitation rate coefficients. Miroplasma excitation using rf at 13.56 MHz has been explored as a method to generate microplasmas at atmospheric pressure in air [20,50,59].

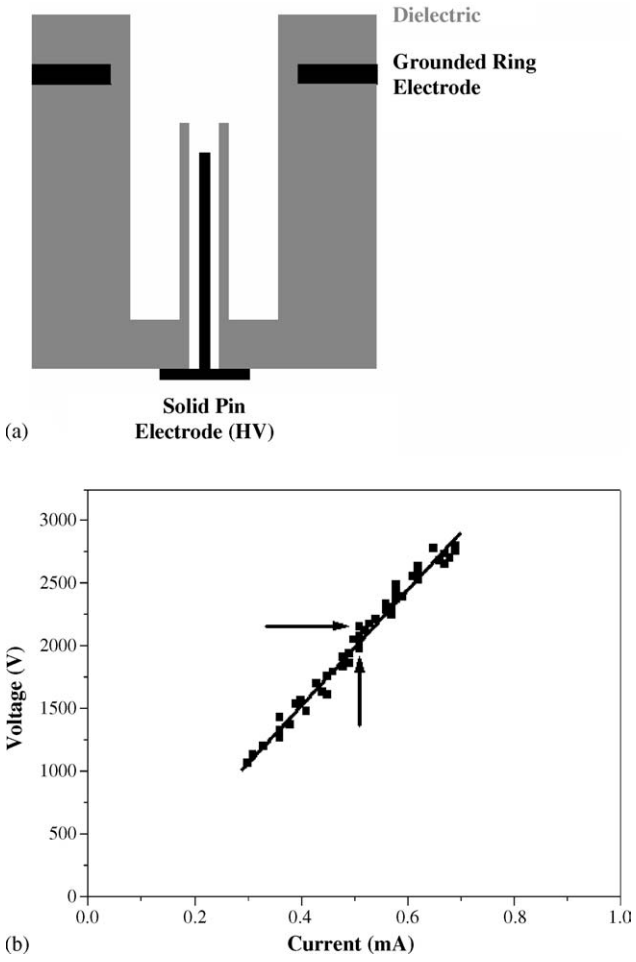

Fig. 4. (a) Schematic diagram of a single-capillary CPE discharge device (not to scale). The solid pin electrode has a diameter of 0.05 mm and is recessed by about 2 mm inside a dielectric tube of 0.2 mm inner diameter. The grounded ring electrode is about 1 mm above the top of the dielectric capillary; (b) current–voltage characteristic of the single-capillary CPE discharge shown in (a). The arrows at a voltage of about 2100 V and a current of about 0.5 mA indicate a point on the *I–V* curve, where the discharge pattern changes from being totally confined inside the capillary to extending beyond the confinement of the capillary.

CPE discharges have been operated at atmospheric pressure in He, Ar, He–N_2, He–air, He–H_2O, N_2–H_2O, and air–H_2O gases and gas mixtures and discharge volumes in arrays of more than 100 cm^3. Current–voltage (*I–V*) characteristics have been obtained for the single-capillary plasma device shown in Fig. 4a excited by ac power in the 10–50 kHz frequency range. As can be seen in Fig. 4b, the *I–V* characteristic over the entire operating range is that of an abnormal glow discharge. The arrows at a voltage of about 2100 V and a current of about 0.5 mA (corresponding to a power of slightly more than 1 W) indicate a point on the *I–V* curve, where the discharge pattern changes from being totally confined inside the capillary to extending beyond the confinement of the capillary. As can be seen in Fig. 4b, there is no indication that this change in the visual appearance of the plasma affects the slope of the *I–V* characteristic.

The C-DBD plasma source is typically excited by rf power at 13.56 MHz [51–54], but in some applications mid-ac frequencies around 400 kHz have also been used [52]. Masoud et al. [52–54] operated their C-DBD in pure rare gases (Ne, Ar) or mixtures containing Ne or Ar with up to 3% additives of molecular gases (H_2, N_2, air). Operating pressures covered the range from a few Torr to about 600 Torr and the electrical power deposited into the plasma ranged from a 5–70 W. While the diameter of the plasma decreases slightly with increasing power (at constant pressure), a drastic change in the visual appearance of the discharge occurs around 60 W in the rare gases or in mixtures that contain predominantly rare gases. The plasma abruptly constricts, which coincides with a drastic increase in the emission intensity from the plasma in the vacuum ultraviolet spectral region [52]. Other plasma parameters also change abruptly (see below).

3.2. Electron temperature and electron energy distribution

Measurements of the electron temperature in rare gas microplasmas have been carried out using emission spectroscopy. Frank et al. [60] obtained an electron temperature of about 1 eV in Ar from line intensity measurements in a dc-driven microdischarge. The electron temperature during pulsed operation was more than twice that value [61]. This increase in the electron temperature, which is correlated to an increase in electron density, is attributed to pulsed electron heating [58]. It is important to realize that measurements which provide information on average electron energies only yield rather low values. The simple fact that microplasmas are efficient sources of excimer radiation points to the presence of a significant fraction of high-energy electrons (with energies exceeding the excitation and ionization energies of the rare gas atoms, i.e., above at least 12 eV in Xe and more than 21 eV in He). Thus, the electron energy distribution function must be highly non-Maxwellian and contain a significant amount of very energetic (“beam”) electrons. Measurements at lower pressures confirm this assumption [62,63]. Badareu and Popescu [62] found evidence of two groups of electrons with mean energies of 0.6 and 5 eV, respectively. Earlier diagnostics studies [64] of the electron energy distribution function (EEDF) in low-pressure HC discharges found copious amounts of electrons with energies well above 10 eV and a tail extending up to the plasma operating voltage. This observation is supported by the fact that Kurunczi et al. [16,65] observed intense Ne_2^* and He_2^* excimer emissions from microdischarges in pure Ne and He, which requires copious amounts of electrons with energies of at least 17 eV in Ne and 21 eV in He. Likewise, the intense Ne_2^* excimer emissions from C-DBDs [52,53] indicate the presence of an appreciable fraction of energetic “beam” electrons in these rf plasmas.

Amorer [41] using a Monte Carlo modeling code predicted relatively high average electron energies of 5–6 eV in CPE discharges operating in the “capillary” mode, which have also been verified experimentally [66].

3.3. Electron density

Electron densities in microplasmas in Ar have been measured using either Stark broadening and shift of the Ar lines around 800 nm [67] or the H Balmer-β line at 486 nm [61]. The

measured electron densities for dc microdischarges were found to exceed 5×10^{14} cm^{-3} and increased slightly with current. When excited by 10 ns pulses of 600 V, the electron densities increased to 5×10^{16} cm^{-3} [61]. Electron densities in these microdischarges in atmospheric pressure air have been measured using heterodyne infrared interferometry and values of up to 10^{16} cm^{-3} were reported [68,69]. The electron densities in CPE discharges and C-DBDs have not been determined accurately to the best of our knowledge.

3.4. Gas temperature

Gas temperature measurements have been performed in rare gas and in air microdischarges using optical emission spectroscopy [68–70] or absorption spectroscopy [71]. The gas temperature in atmospheric pressure air microplasmas was measured to be in the range from 1700 to 2000 K for discharge currents between 4 and 12 mA by evaluating the rotational (0, 0) band of the second positive N_2 system [68,69]. By contrast, the temperature in a Ne microplasma at 400 Torr was only around 400 K [72] at a current of 1 mA. The temperature was obtained from the analysis of the N_2 band system (using a trace admixture of N_2 added to the Ne). Absorption spectroscopy (Doppler broadening of Ar lines) was used by Penache et al. [67] to determine the gas temperature in Ar microdischarges and they observed an increase with pressure from 380 K at 50 mbar to 1100 K at 400 mbar. This result indicates that the gas temperature depends strongly on the nature of the gas, on the pressure and perhaps also on the geometry of the microcavity in which the microplasma is generated. In general, gas temperatures are highest for molecular gases, such as air and significantly lower for rare gases.

Recently, a spectroscopic analysis of the emission of the unresolved N_2 second positive band system from a single-capillary CPE discharge plasma in atmospheric pressure air was carried out [71]. Measurements were done for various discharge powers in a geometry, where the emissions from inside the capillary, presumably the hottest part of the plasma, were analyzed. The results shown in Fig. 5 reveal rotational temperatures in the plasma inside the capillary rising from about 340 to 530 K at the highest power level studied. Note that the rate of temperature increase with increasing power is fairly rapid at lower powers where the plasma is confined inside the capillary, but changes to a more gradual increase at higher power levels where the plasma extends beyond the confinement of the capillary.

Masoud et al. [53] carried out extensive studies of the rotational and vibrational temperatures in C-DBDs in Ne by analyzing emissions from the N_2 2nd positive systems arising from minute (<0.05%) N_2 admixtures to the Ne feed gas. At a constant power of 30 W, the gas temperature remained essentially constant around 350 K between 200 and 600 Torr. At a fixed pressure of 400 Torr, the gas temperature increased essentially linearly with input power from 350 K at 25 W to 390 K at 60 W. This was attributed to a (slight) gas heating as the power input into the plasma increases. Above 60 W, the temperature jumped abruptly to more than 420 K. This jump in the gas

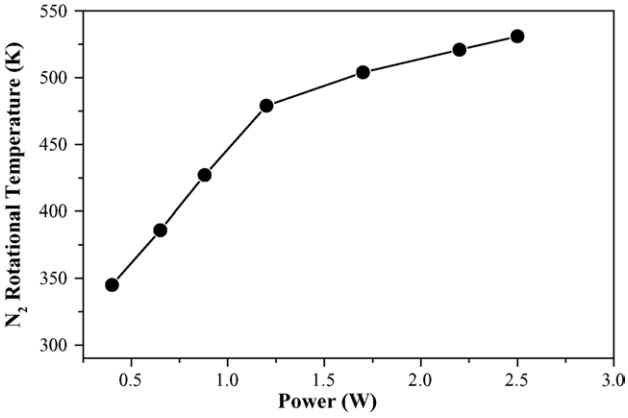

Fig. 5. Rotational temperatures of N_2 in the single-capillary CPE discharge shown in Fig. 4a in atmospheric pressure air. The rotational temperatures were obtained from an emission spectroscopic analysis of the N_2 second positive system emitted along the direction of the capillary axis.

temperature coincided with the previously mentioned change in the visual appearance of the plasma at this power level and the appreciable increase in the intensity of vacuum ultraviolet emissions from the plasma. The vibrational temperatures measured by Masoud et al. [53] showed a decrease with pressure between 200 and 600 Torr from 3030 to 2270 K (at constant power). This was attributed to a combination of an enhancement in the collisional relaxation of the vibrationally excited N_2 levels as the collision frequency increases (with increasing pressure) and a decrease of the electron temperature with pressure. At constant pressure (400 Torr), the vibrational temperature was found to increase with increasing power deposition into the plasma, from about 2500 K at 20 W to 2950 K at 60 W. This increase is a consequence of the increase in the electron temperature with power, which facilitates a more efficient excitation of the higher lying vibrational levels of N_2 by the plasma electrons.

4. Modeling of microplasmas

Microplasma and microdischarge devices have been widely used in applications for more than 10 years. During that time, our ability to understand and model the basic mechanisms that generate these microplasmas and explain their remarkable stability has been slow to catch up. It has only been in the past few years that results of modeling and computational investigations of microdischarge devices have emerged in the literature and helped shed light on the basic understanding of microplasmas. It is not the purpose of this topical review to describe in detail the results of these modeling efforts. Here we simply summarize some of the important general insights gained from the modeling and refer the interested reader for further details to the recent publications of Kushner [13] and Boeuf et al. [72,73], which contain many additional references to earlier work.

Much of the modeling efforts have concentrated on the original geometry as depicted in Fig. 2a and other similar cylindrically symmetric structures with a central hole through a metal–dielectric–metal sandwich stack, often with slightly con-

ical central holes. The small dimensions and resulting high operating pressures of microdischarges allow these devices to operate in regimes that are inaccessible to conventional macroscopic devices. Power depositions of more than 10 kW/cm^3 are not uncommon in cw-excited microdischarges, whereas such values can be realized in macroscopic discharges only with pulsed power. The resulting high current densities in microdischarges lead to significant gas heating and large momentum transfer from the electrons to the gas, which initiates gas dynamics that cause – among other phenomena – gas rarefaction. Microdischarge operation may result in a situation where the device dimensions are comparable to the Debye length, which may impact the ability of the discharge to utilize the full electrode geometry [13].

For a microdischarge operating in 250 Torr Ar at currents between 0.5 and 10 mA, model predictions for the electrical properties (potential, electric fields), plasma properties (electron temperature of the slow bulk electrons and the fast beam electrons, electron sources, electron density), and species densities (Ar ground-state, Ar (4s), Ar (4p), and Ar_2^* excimers) were found to be in satisfactory agreement with experimental data. The microdischarge was found to be particularly sensitive to the secondary electron emission coefficient for ions and, in some cases, also for photons. Contributions to the ionization balance arising from the beam electrons, which result from secondary electron emission, and are accelerated in the cathode fall determine the operating characteristic of the microdischarge device critically.

5. Applications of microplasmas

Microdischarges and microplasmas have made an enormous impact on applications. The diversity of applications, in which microplasmas are being employed renders it impossible to provide a detailed account of all microplasma applications in this article. Therefore, we have selected a few applications on topics that we feel are most relevant to the audience of this journal and discuss them in more detail below. Two very good sources for further information on microplasma applications are the recent J. Phys. D Cluster Issue on Microplasmas (volume 38, 2005) and Ref. [11]. Both sources contain a large number of references to other microplasma applications.

5.1. Microplasmas for environmental applications

Non-thermal plasma devices have been used in numerous environmental applications such as NO_x and SO_x remediation and the destruction of volatile organic compounds (VOCs) for more than 20 years (see e.g., Penetrante and Schultheiss [74]). High-energy electron beams, corona discharges, dielectric barrier discharges, and various surface-type discharges, sometimes with packed beds of ferroelectric pellets, have been widely utilized discharge configurations for the generating non-thermal plasmas in the environmental field.

Koutsospyros and co-workers [75–77] carried out comprehensive studies of VOC destruction in the context of exploring the use of non-thermal microplasmas for use in advanced life support (ALS) systems designs for controlled cabin environments (submarine, aircraft, spacecraft, and space station). The destruction of several prototypical aliphatic (ethylene, heptane, octane) and aromatic (benzene, toluene, ethylbenzene, xylene) compounds as well as ammonia were studied. Initial contaminant concentrations varied between 75 and 1500 ppm(v) (parts per million in volume) in ambient air with comparatively low gas flow rates between 1 and 10 l per minute (l/min), which are typical for ALS systems. Destruction efficiencies were determined as a function of plasma energy density, initial contaminant concentration, residence time in the plasma volume, reactor volume, and single contaminant versus contaminant mixture and a kinetic model was developed to determine the relevant rate constants for contaminant destruction. Koutsospyros et al. used the three microplasma reactors based on the CPE discharge (see Fig. 6). The first reactor is of a rectangular design with solid pin electrodes and a gas flow direction that is perpendicular to the axes of the capillaries (cross-flow or CF-CPE reactor). The reactor consists of two parallel dielectric plates separated by a 3.2 or 1.6 mm gap. One of the plates is perforated with 100 capillaries of 0.4 mm diameter each. The cathode consists of metallic pins that are partially inserted into the capillaries to minimize energy losses in the system and to improve plasma generation and stability.

A second rectangular plasma reactor uses hollow pin electrodes and is operated in the flow-through regime, where the gas stream is introduced through the hollow pin electrodes and the capillaries (FT-CPE reactor). This design maximizes the exposure of the contaminants to the region of highest plasma density. A total of 37 pins of 0.8 mm diameter were used in an effort to minimize the pressure drop through the system when the gas flows through the hollow pins. Lastly, an annular (A-CPE) reactor, whose body is made of Pyrex was used. One electrode consists of an Al screen that surrounds the Pyrex cylinder, whereas the other electrode is a metal bar placed concentrically inside the glass cylinder and covered with a perforated alumina silicate dielectric layer. The contaminant streams flows axially through the reactor. This mode of operation allows the contaminated gas stream to flow through the entire annulus of the reactor where exposure to the plasma occurs. The overall dimensions of the reactor were 254 mm in length with a 38 mm outer diameter.

Input powers ranging from 10 to 100 W were used to generate plasma volumes between 3 and 20 cm^3. This resulted in energy densities (J/cm^3), defined as electrical input power (W) divided by the gas flow rate entering the plasma reactor (cm^3/s), between 0.5 and 10 J/cm^3 and residence times in the range of 0.2–2 s. For all compounds, operating conditions could be identified that guaranteed destruction efficiencies of 95% and higher; in many cases complete destruction (within the detection limits) could be obtained. Fig. 7, as an example, shows the destruction efficiency for benzene in two CPE plasma reactors, an annular reactor and a cross-flow, solid pin electrode reactor. As can be seen, essentially complete destruction can be achieved in the annular reactor for specific energies of 3 J/cm^3 and above. On the other hand, specific energies approaching 10 J/cm^3 are required to achieve a comparable destruction efficiency in the cross-flow reactor. This indicates that optimization of the reactor geometry

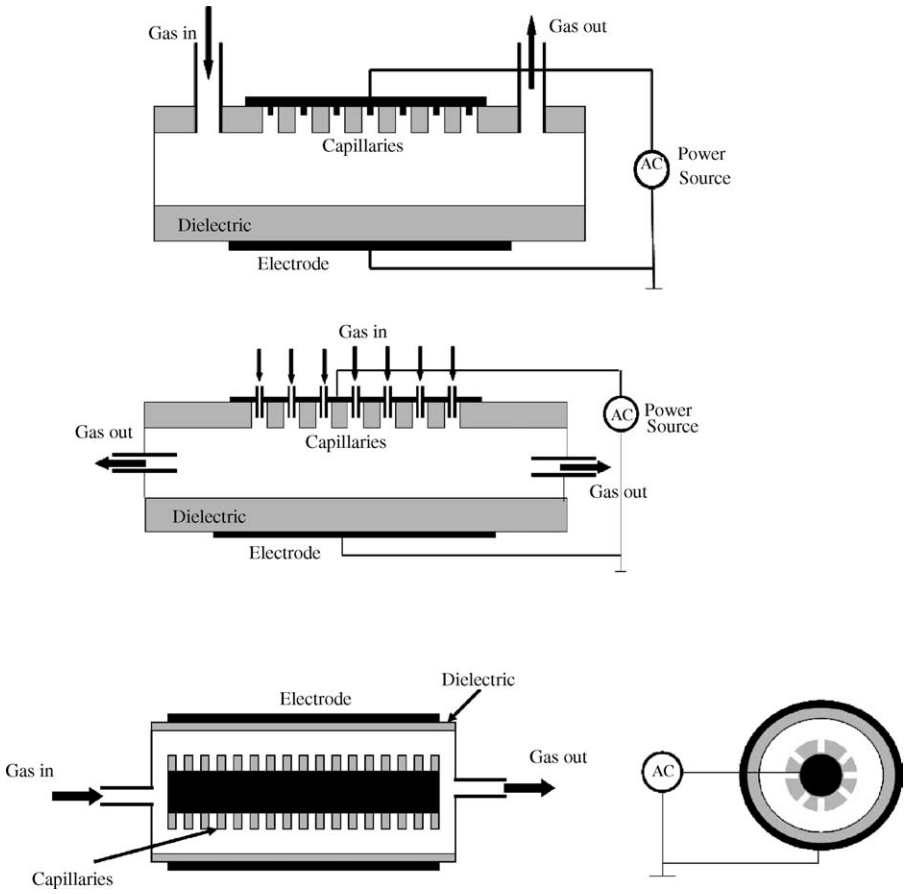

Fig. 6. Schematic diagram of a three capillary plasma electrode (CPE) discharge configurations used in reactors for environmental applications. Top: cross-sectional view of a cross-flow CPE (CF-CPE) reactor with solid pin electrodes; center: cross-sectional view of a flow-through CEP (FT-CPE) reactor with hollow pin electrodes; bottom: two cross-sectional views of an annular CPE (A-CPE) reactor with a solid center electrode.

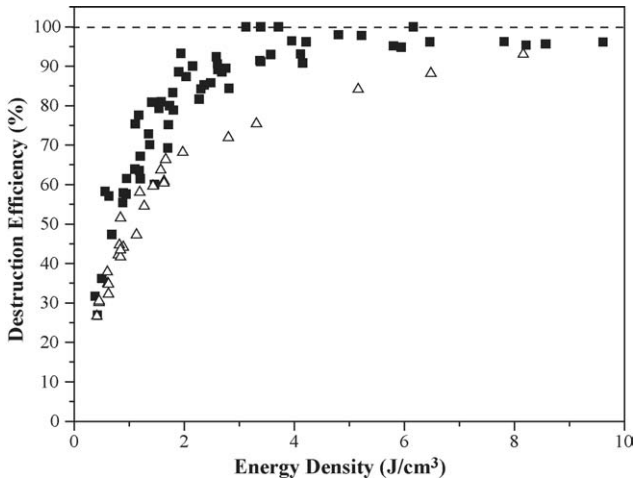

Fig. 7. Benzene destruction efficiency in an annular CPE plasma reactor (solid squares) and in a cross-flow CPE plasma reactor (open triangles). For both reactors, data are shown for initial contaminant concentrations varying between 200 and 1200 ppm(v) and flow rates varying between 2 and 8 l/min; in all cases, the residence was chosen to be sufficiently long to ensure maximum destruction efficiency.

is a critical component in achieving maximum destruction efficiencies. The results of the extensive parametric studies reported by Koutsospyros and co-workers can be summarized as follows:

1. Maximum VOC destruction efficiencies between 95 and 100% were obtained for all compounds studied (for the right, compound-dependent combination of specific energy, residence time, and reactor geometry).
2. The VOC destruction efficiency increased with the specific energy initially, but leveled off at values of the specific energy that are compound-dependent; a similar finding holds for dependence of the VOC destruction efficiency on the residence time.
3. The destruction efficiency increased with increasing initial contaminant concentration, i.e., dilute waste streams are more difficult to treat efficiently.

The maximum destruction efficiency, however, is only one aspect of the VOC destruction process. The formation and characterization of by-products is another important consideration. Ultimately, one needs to measure the concentrations of all identified by-products and the gaseous carbon oxides, CO and CO_2 to obtain "carbon closure." Carbon closure can be determined by evaluating the carbon mass balances for the reactants and all

identified products. If contaminants and products are measured in ppm(v), the contribution of each component to the carbon concentration (measured in $\mu g/cm^3$) can be expressed as:

$$C_{C(i)} = \left[\frac{(pM_i)}{RT}\right] C_i r \quad (1)$$

where $C_{C(i)}$ denotes the carbon concentration contributed by component i, p refers to the pressure, M_i, the molar mass of component i, R, the universal gas constant, T, the absolute temperature, C_i refers to the concentration of compound i, and $r = M_C/M$ denotes the carbon mass content per mole of compound i. The resulting product carbon is obtained by adding the carbon concentrations of the unreacted hydrocarbons, CO, and CO_2 using the above equation. Carbon closure is then computed by taking the ratio of the product carbon to the influent carbon. Carbon closure for benzene and ethylene was essentially 100%, which indicates that all influent carbon is accounted for in the form of identified final products, CO, and CO_2. Carbon closure for toluene, heptane, octane, and ethylbenzene ranged from 70 to 90%. Although no attempt was made by Koutsospyros and co-workers [75–77] to identify and quantify all by-products, the gap between reported carbon closure values and 100% is most likely due to the formation of low mass chain hydrocarbons, alcohols, and aldehydes [78–80].

5.2. Biological applications of microplasmas

The interaction of plasmas with biological systems falls generally into two areas. Most of the work has been focused on applications such as inactivation, bio-decontamination, and sterilization, where lethal plasma intensities are applied to initiate cell death. Some work has also been done in which a non-lethal plasma dosage was used to change the cell response in a controlled way [81].

The inactivation of individual microorganisms by plasmas has received much attention in recent years [82–96]. Particular emphasis has been on the utilization of atmospheric pressure plasmas as they do not require operation in costly vacuum enclosures and thus facilitate the convenient and low-cost treatment of large surface areas. Spore-forming bacteria, in particular bacteria of the genera *Bacillus*, are among the most resistant individual microorganisms. The species *Bacillus subtilis* has received particular attention, as these bacteria are easy to grow in a reproducible fashion under chemically well-defined conditions and are considered a non-lethal surrogate for the lethal *Bacillus anthracis*, which causes anthrax.

A commonly used measure for the effectiveness of a decontamination method is the so-called *D*-value (decimal reduction factor), which is the time that it takes to reduce a certain concentration of active microorganisms by one order of magnitude. In the case of *Bacillus subtilis* spores, typical *D*-value for conventional inactivation methods such as the use of dry or steam heat or chemicals such as ethylene oxide (EtO) or chlorine dioxide (ClO_2) are in the range of a few minutes [94]. Plasma-based inactivation using non-equilibrium plasmas can achieve similar *D*-value (see below and Refs. [95] and [96]) with the added advantages that heat-sensitive material can be decontaminated and without generating environmentally hazardous, contaminated chemicals as by-products.

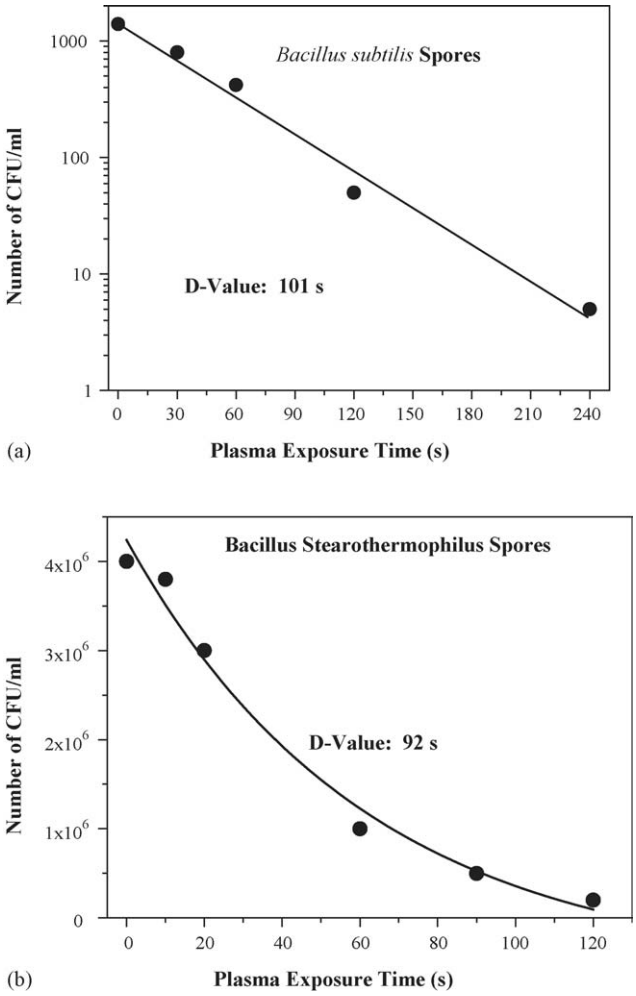

Fig. 8. (a) Inactivation of *Bacillus subtilis* spores in an atmospheric pressure CPE plasma reactor in air. The number of colony forming units (CFU)/ml is plotted vs. the plasma exposure time. The solid line represents a single-exponential decay curve through the data points. The corresponding *D*-value is 101 s. (b) Same for the inactivation of *Bacillus stearothermophilus* spores in a He plasma. The solid line represents a single-exponential decay curve through the data points. The corresponding *D*-value is 92 s.

Panikov et al. [39] studied the inactivation of several spore-forming bacteria using atmospheric pressure CPE plasma reactors in various gas mixtures (pure He, He–N_2, He–air, dry air, and humid air). Fig. 8 shows the results of the plasma-initiated inactivation of *Bacillus subtilis* spores (Fig. 8a) and *Bacillus stearothermophilus* spores (Fig. 8b). The following observations are noteworthy:

1. The inactivation curves in both cases are well described by a single-exponential decay law.
2. *D*-value of slightly less than 2 min can be achieved for some of the more resistant spore-forming bacteria; the corresponding *D*-value for the inactivation of bacteria in the vegetative state are significantly shorter [85,94-96].
3. The single-exponential decay holds for high initial spore concentrations (>10^6 colony forming units (CFU) per ml) as well

as for dilute concentrations (<10^4 CFU/ml); likewise, the *D*-value are concentration independent.

4. The single-exponential decay behavior extends to longer times and covers many orders of magnitude of cell reduction [95,96].

The above observations are consistent with results obtained by other researchers using other types of high-pressure plasmas and a variety of bacteria. By contrast, the use of low-pressure plasmas for the plasma-initiated inactivation of bacteria tends to result in more complicated decay curves that often require two (or even more) exponential decay constants, which dominate in different time regimes [90–92]. This has been attributed to the presence of several cell kill mechanisms (plasma-generated heat and UV radiation, radicals, ions), which may cause the cell death on different time scales. The observed single-exponential decay in the case of high-pressure plasmas may point to the dominance of a single cell kill mechanism or may be indicative of the fact that the various cell kill mechanisms contribute with similar time constants in a high-pressure plasma.

Recently, first reports regarding the plasma-initiated inactivation of biofilms have appeared in the literature [77,97]. Biofilms are highly structured communities of bacteria with complex structures that can adhere to surfaces and interfaces. Biofilm formation is initiated when planktonic bacteria adhere to surfaces and begin to excrete exopolysaccharide that can anchor them to the surface. Many serious side effects associated with illnesses and the rejection of implants are often attributed to biofilms. Likewise, biofilms impact adversely on many industrial processes and have unwanted effects on process efficiencies and on end-product purity. Among the most notable differences between planktonic cells and biofilms is the much higher resistance of biofilms to antibiotics, germicides, and other conventional sterilization and inactivation methods.

Initial results using a DBD plasma and *C. violaceum* biofilm-forming cells [77,97] indicate a slower and more complex inactivation process compared to individual bacteria. The number of biofilm-forming cells was found to be reduced rapidly by more than two orders of magnitude after a plasma exposure of 5 min, but it took almost another 60 min of plasma exposure to achieve a significant further reduction of the CFU count. The overall CFU reduction after 60 min reported in [77] and [97] was about 3–4 orders of magnitude.

5.3. Microdischarges as vacuum ultraviolet (VUV) and ultraviolet (UV) radiation sources

The presence of a significant number of energetic "beam" electrons in the electron energy distribution functions of all microplasmas in conjunction with the stable operation of these discharges at high pressure favors three-body collisions, and thus enables processes such as ozone generation and excimer formation. The latter effect has been extensively studied for the rare gases He [17,22,67,98–103] and for some rare gas halide mixtures which generated ArF excimer radiation [99,104]. Efficiencies of up to 8% have been reported for Xe excimer formation in microplasma sources [102,105], lower efficiencies for heavier rare gases [99]. For rare gas halide mixtures, efficiencies of the order of a few percent have been measured.

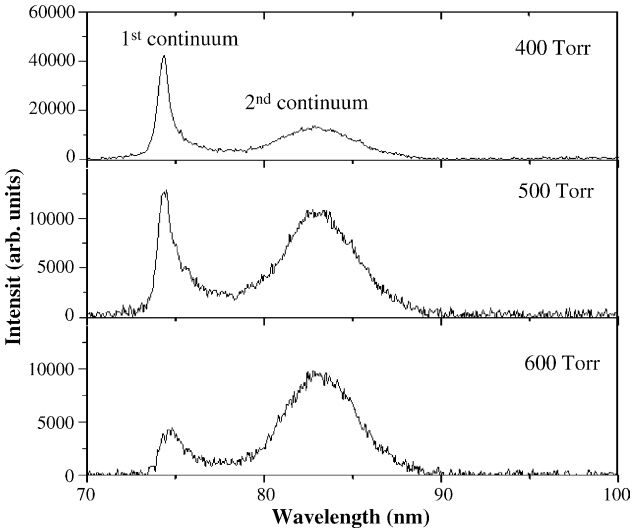

Fig. 9. High-pressure emission spectrum a pure neon C-DBD at 400, 500 and 600 Torr. The net rf power is 30 W and the gas flow rate is 800 sccm.

In addition to being efficient sources of excimer radiation microplasmas in various geometries have also been shown to emit atomic line radiation with high efficiency. Kurunczi et al. [16] and Masoud et al. [52] observed intense emission of the atomic hydrogen Lyman-α (121.6 nm) and Lyman-β (102.5 nm) lines, from respectively, a high-pressure microcavity plasma and a C-DBD in Ne with a small H_2 admixture. Fig. 9 shows the Ne_2^* excimer emissions (1st and 2nd continuum) from a C-DBD plasma at various pressures in pure Ne. Fig. 10 shows the emission spectrum from a 500 Torr Ne plasma with 0.02% H_2 admixture. The Ne_2^* excimer emissions have essentially disappeared and the spectrum is dominated by the H Lyman-α line. Only a very weak indication of the Ne_2^* first excimer contin-

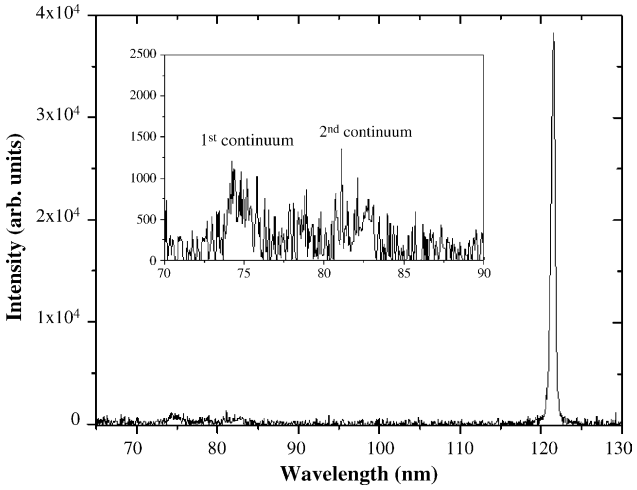

Fig. 10. Emission spectrum from a neon C-DBD with a small admixture of hydrogen (0.02%) at a total pressure of 500 Torr, a flow rate of 800 sccm and a net rf power of 30 W. The inset shows the expanded view of the spectrum in the 70–90 nm region.

uum remains as shown in the insert. The Lyman-α emission can be attributed to the presence of (at least) two processes, the near-resonant energy transfer from Ne_2^* to H_2:

$$Ne_2^*(^3\Sigma_u) + H_2 \rightarrow 2Ne + H(n=1) + H^*(n=2) \quad (2a)$$

$$H^*(n=2) \rightarrow H(n=1) + h\nu(\text{Lyman-}\alpha,\ 121.6\,\text{nm}) \quad (2b)$$

and the dissociative recombination (DR) of H_2^+, which is the result of the Penning ionization (PI) of H_2:

$$Ne_2^*(^3\Sigma_u) + H_2 \rightarrow 2Ne + H_2^+ + e^- \quad (3a)$$

$$H_2^+ + e^- \rightarrow H(n=1) + H^*(n=2) \quad (3b)$$

$$H^*(n=2) \rightarrow H(n=1) + h\nu\,(\text{Lyman-}\alpha,\ 121.6\,\text{nm}) \quad (3c)$$

We note that reaction (3b) has a branching ratio of about 0.1–0.2 depending on the exact conditions in the discharge and competes with two other recombination processes which do not lead to the emission of a 121.6 nm photon:

$$H_2^+ + e^- \rightarrow 2H(n=1)\,(\text{branching ration about } 0.8\text{–}0.9) \quad (3d)$$

$$H_2^+ + e^- + M \rightarrow H_2 + M\,(\text{branching ration very small},\ < 0.05) \quad (3e)$$

Other atomic line emissions that have been observed include various N lines from microplasmas in Ar–N_2 [54] and Ne–N_2 mixtures [106] and the emission of strong O lines at 130.2 and 130.5 nm from a microplasma in an Ar–O_2 mixture [101,102]. The latter process can be attributed to the near-resonant absorption of an Ar_2^* excimer photon by the O atoms that are produced in the plasma by dissociation of O_2.

5.4. Microplasmas for gas and surface analysis

The first use of plasmas for chemical analysis purposes goes back to Bunsen and Kirchhoff, who employed flames, which are low-density near-thermal plasmas at atmospheric pressure. The first mass spectrometer, the parabolic spectrograph, constructed by Thomson [107], can be viewed as a plasma application, because it used a low-pressure glow discharge as ion source. Later spark and arc plasmas were used as light sources and ion sources in optical and mass spectrographs and spectrometers. The development of ion sources initially focused on electron-impact sources operated at very low pressure, which was done for reasons of convenience because of the required high vacuum inside the mass spectrometer. Because of the possible electron-impact-induced fragmentation of the molecule under study by the electrons, problems were incurred in the unambiguous identification of the target molecule, particularly in the case of more complex molecules. This shortcoming was addressed by using chemical ionization in a high-pressure plasma, which avoid the strong decomposition of the molecule by replacing the electron-impact-induced ion formation by a process that is based on the attachment of H^+ ions (protons).

Some selected examples of microplasmas used in analytical devices are discussed in more detail below.

5.4.1. Gas analysis

5.4.1.1. dc plasma sources. Miclea and co-workers [67,108,109] used a microcavity plasma at atmospheric pressure as a promising miniaturized ionization source for mass spectrometry and optical spectrometry also. The microplasma jet source consists of a sandwich metal/insulator/metal structure with a central hole of 100–300 μm diameter. The thickness of the insulator (Al_2O_3) is about 100 μm. Various electrode materials were used, primarily Cu and Pt. The Pt electrodes have a four times longer lifetime than Cu because of the lower sputter rate. The ignition voltage varies between 400 and 700 V resulting in sustaining voltages between 200 and 300 V. The power density that can be achieved is about 1 MW/cm^3 for an input power of 1 W. The discharge operates at atmospheric pressure, primarily with He as the carrier gas, in two modes. The static mode is characterized by the same pressure at both electrodes. In the jet mode, atmospheric pressure is maintained on the anode side with a much lower pressure (0.2 mbar) on the cathode side. The jet mode is preferred for mass spectrometry, while the static mode is more suitable for optical spectrometry. Because of the small absorption length in the microcavity plasma, the device is more suited for emission spectroscopy than for absorption spectroscopy [109]. For mass spectrometric applications, the analyte samples are introduced into the He gas flow. Detection limits for halogenated organic compounds in the order of pg/s were observed. In the case of ferrocene, a detection limit of about 500 ppb for Fe was reported [109]. The authors realized limitations for the use of microdischarges for analytical purpose: (i) the small size of the microstructure causes the dissociation of the analyte to be incomplete, (ii) the analysis of liquid samples will be difficult or impossible, and (iii) the lifetime of the microstructure is limited due to thermal stress or sputtering of the cathode.

Jost et al. [110] used a small-volume corona discharge as an ion source in air in an atmospheric pressure chemical ionization mass spectrometer (AP-CIMS) where the ions from sample gases are formed by ion molecule reactions. The corona discharge operates at 5 kV dc with a discharge current of about 5 μA, which is limited by a resistor of 1000 MΩ. Peng et al. [111] also employed an atmospheric pressure corona discharge as the ion source in a mass spectrometer. These authors used diode laser desorption of analyte molecules dissolved by thin layer chromatography for species identification purposes.

Eijkel et al. [112,113] developed an optical emission detector that uses a dc He microdischarge (at 130 Torr) in a long, narrow plasma chamber with a volume of only 50 nl with an electrode at each end for molecular fragmentation and excitation. The device is constructed on a glass chip. The dimensions of the plasma chamber are 2000 μm (length) × 250 μm (width) × 100 μm (height) or alternatively, 1000 μm × 350 μm × 150 μm. The gas inlet pressure is 750 Torr, while there are vacuum conditions at the outlet. The light emission is analyzed by a photomultiplier tube coupled to a bundle of quartz fibers placed directly on top of the plasma chamber. Cathode sputtering is limiting the lifetime of the device to about 2 h. This device was used for the detection of methane by observing the emission of the CH radical with a

detection limit of 3×10^{-12} g/s (600 ppm). A microdischarge in a 180 nl plasma chamber with a He gas flow (860 Torr, 320 nl/s) was tested successfully as detector for gas chromatography of hydrocarbons (hexane/800 ppb and several alcohols).

5.4.1.2. RF plasma sources. The utility of dielectric barrier discharges for analytical purposes was investigated by Miclea and co-workers [114–116]. A plasma column was generated by two electrodes (coated by dielectric layers of 20 μm), 50 mm long and 0.7 mm wide with a gap of 1 mm. The discharge operated in He or Ar (10–100 hPa, 1000 ml/min) with a rectangular voltage of 5–20 kHz and a peak-to-peak voltage of 400–900 V. Halogenated and sulfur-containing hydrocarbons were investigated by element-selective diode laser absorption spectroscopy using the good absorption properties of the "long" plasma column with detection limits in the pg/s range.

A plasma column of similar geometry can be generated as a capacitively coupled 13.56 MHz discharge in a 200 μm × 500 μm channel with the length of a few centimeters in a quartz wafer [117]. The parallel plate electrodes are positioned on the outer bottom of the quartz plate that contains the plasma channel and on the outer surface of the upper quartz plate. This atmospheric pressure discharge has great potential as a detector for a miniaturized gas chromatography system. The plasma has no contact with the electrodes as in dc systems [112,113] and, therefore, there is no possibility of contamination by electrode materials. A miniature capacitively coupled (20 kHz) plasma inside a thin silica tubing (inner diameter 250 μm) between two metallic electrodes was developed for the detection of non-metals in organic compounds by gas chromatography [118]. Detection limits of e.g., 0.3 pg/s for Br and 0.1 pg/s for Cl were presented.

Another example of a capacitively coupled RF microdischarge is the atomic emission source in a gas chromatography detector [119]. The discharge is sustained by RF voltage and operates between two disk-shaped metallic electrodes separated by a sapphire disk. This arrangement corresponds to a microdischarge in hollow-cathode geometry. The samples are introduced with a He gas flow into the central orifice inside the electrodes and the insolating sapphire disk. The point-like plasma is formed inside the orifice (diameter 15 μm, height 550 μm). For hexachlorocyclohexane, a detection limit of 8.5 pg and at least three orders of magnitude of linear range were observed.

All the plasmas described here as GC detectors were sources for optical emission spectroscopy or were operated as targets in optical absorption spectroscopy. Brede et al. [120] applied a capacitively coupled discharge at 350 kHz in a 0.35 mm (inner diameter) fused silica capillary of 3.5 cm length as an ion source for a quadrupole mass spectrometer. The detection limit of 2.2 pg/s for Cl is comparable with the values of optical emission spectroscopy.

Inductively coupled plasmas were also successfully applied in microplasma sources for analytical purposes. Minayeva and Hopwood [121] developed an inductively coupled plasma source (operating at 0.1–10 Torr) with a planar three-turn inductor and a plasma chamber of 3 mm radius and 6 mm length. The operating frequency is 493 MHz and the power transmitted to the plasma is 0.75–3.5 W. The plasma is observed radially through 1 mm thick quartz windows by optical emission spectroscopy. For SO_2, a detection limit of 45 ppb was determined.

5.4.1.3. Microwave plasma sources. A low power microwave plasma source for atomic emission spectroscopy was developed by Bilgic and co-workers [122–124]. A small channel with a cross-section of 1 mm^2 and a length of 20–30 mm inside a fused silica dielectric wafer serves as the plasma chamber. The electrodeless discharge is excited by a strip-like antenna coupled via a matching element to a microwave power supply (2.45 GHz). The discharge operates at atmospheric pressure with an Ar gas flow of 50–1000 ml/min and a microwave input power of 10–40 W. The application of sapphire substrates with its permittivity enables the use of He. The optical emission is observed in axial direction. Quantitative analyses of Hg and Cl confirm the capability of this device as detector in gas chromatography.

Another interesting application of a microwave-excited microplasma was presented by Siebert et al. [125]. A mass spectrometer fabricated as a microsystem is used as a mass filter that combines velocity selectivity with principles of time of flight and trajectory stability. A noble gas (80 Pa) in the plasma chamber is excited by microwaves in the power range from 100 to 350 mW and serves as electron source instead of a filament. Electron currents up to 100 μA were extracted from the plasma and were accelerated into the ion source. The dimensions of the entire mass spectrometer are only a few cm^3.

5.4.2. Surface treatment

The applicability of microdischarge to surface treatment is developing rapidly and covers both the use of the single microdischarges for the treatment of selected sites, e.g., for the production of microstructures and the use of microdischarge arrays. The treatment of 3-D will soon become possible. Ichiki et al. [126] described a miniaturized rf-driven (100 MHz, 150–300 W) inductively coupled plasma jet source consisting of a 1 mm inner diameter discharge tube with a 0.1 mm diameter nozzle at one end. An argon plasma jet (flow rate 6–10 slm) with admixtures of halogen gases was successfully used for drilling of holes with diameters of several 100 μm in silicon wafers with etch rates of 4000 μm/m. A plasma jet generated in a capillary by a capacitively coupled rf discharge with two outer electrodes or one inner electrode was tested in connection with the enhancement of the surface energy of bipolar oriented polypropylene foils, plasma-enhanced CVD of silicon–organic compounds, plasma cleaning, plasma activation, and biomedical appliances [55].

A microplasma source, the so-called plasma needle, has also been used in the treatment of dental cavities [127]. A microplasma is generated at the tip of a thin tungsten wire (0.3 mm diameter). The tungsten wire is moveable in a glass capillary, so that a variable length extends outside the capillary. The capillary is centered inside a Perspex tube of 4 mm inner diameter, through which He as a feed gas is delivered at a flow rate of 2 l/min. The discharge is powered by a rf voltage at 13 MHz. This plasma needle was tested for cleaning and

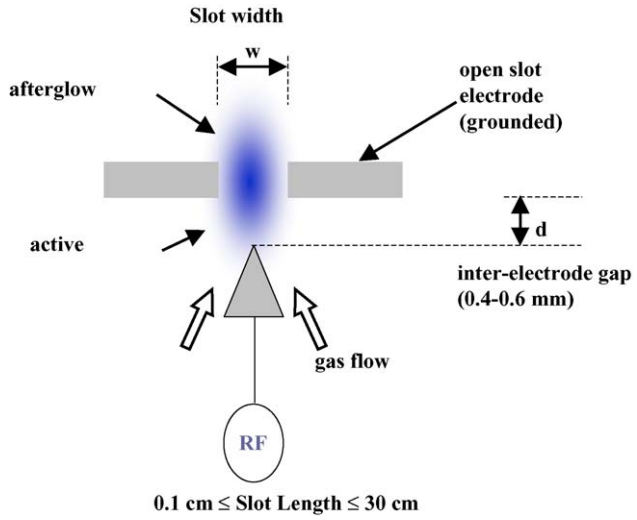

Fig. 11. Atmospheric pressure open-air hollow slot microplasma source [128].

sterilization of infected tissue in dental cavity without thermal stress.

A linear microplasma source was developed by Rahul et al. [128], which uses atmospheric pressure air in an open hollow slot configuration with a grounded slot of width 50–800 μm and a wedge at a distance of 100–600 μm (Fig. 11). The wedge and the slot electrodes are variable from 1 to 30 cm in length. For a length of 7.5 cm, typical flow rates of He and Ar were 1–20 slm. The discharge operates at 13.56 MHz and the active plasma between the wedge and the slot electrodes is diffuse and not filamentary up to a current of 1.5 A per cm slot length. The afterglow region behind the slot was used for surface treatment of polymers as well as for bacterial inactivation.

Surface treatment of polypropylene foils was reported using a scalable plasma source constructed of microcavity arrays [129]. The overall surface area of the source is 40 mm × 320 mm with the diameter of each microdischarge being 0.2 mm and a coplanar electrode geometry with an interelectode distance of 0.5–1.0 mm. The source is operated at 13.56 MHz in He or Ar with small admixtures of O_2 or N_2 at pressures between 100 mbar and atmospheric pressure. The power density can be varied over a wide range from 0.1 to 20 W/cm^2. A treatment time of 3 s results in a reduction of the initial water contact angle of polypropylene from 90 to 30° (Ar plasma) or 45° (He plasma).

6. Summary and outlook

Microdischarges and microplasmas are characterized by plasma dimensions below 1 mm and operating pressures up to and exceeding atmospheric pressure. In such devices, plasma–surface interactions become increasingly important due to the increase of the surface area-to-volume ratio. Microdischarges operating as glow discharges are dominated by processes in the cathode fall to a much larger extent than macroscopic glow discharges. As a consequence, plasmas at low gas temperatures can be generated with electron energy distributions, which contain large fractions of high-energy electrons. High-pressure operation in conjunction with an abundance of high-energy electrons favors three-body reactions such as excimer formation. The energy losses to the surfaces surrounding the plasma contribute to an enhanced plasma stability.

Microdischarges have allowed us to generate stable glow discharges in a wide variety of gases at atmospheric pressure. Electron densities in dc microdischarges have been found to be on the order of 10^{15} cm^{-3}, gas temperatures range from values close to room temperature to approximately 2000 K and are generally lower for noble gases and higher for molecular gases. This is still an emerging field and it appears that the widespread adoption of microfabrication technology and nanostructures will facilitate the development of unique devices. New applications are emerging rapidly and our ability to understand and model the underlying basic processes is gaining momentum. While perhaps driven initially by the potential for novel applications, the pursuit of microplasmas affords the possibility to explore new realms of plasma science at *pd* values that are comparable to those for large-volume, low-pressure plasmas.

Acknowledgments

We would like to acknowledge helpful discussions with many colleagues over the past few years. The results presented in this article are based in part on research supported by the U.S. National Science Foundation (NSF), the U.S. Air Force Office of Scientific Research (AFOSR), the U.S. Army Research Office (ARO), and the U.S. National Aeronautics and Space Administration (NASA). One of us (KB) would like to acknowledge the hospitality of Prof. F.A. Gianturco, University of Rome during the final stages of the preparation of this manuscript.

References

[1] M. Faraday, Experimental Researches in Electricity, vol. I, Taylor and Francis, London, 1839.
[2] M. Faraday, Experimental Researches in Electricity, vol. II, Taylor and Francis, London, 1844.
[3] M. Faraday, Experimental Researches in Electricity, vol. III, Taylor and Francis, London, 1855.
[4] I. Langmuir, Proc. Natl. Acad. Sci. 14 (1926) 627;
see also L. Tonks, I. Langmuir, Phys. Rev. A 33 (1929) 195.
[5] C.T.R. Wilson, Proc. Phys. Soc. London 68 (1901) 151.
[6] J.S. Townsend, H.E. Hurst, Phil. Mag. 8 (1904) 738.
[7] J.S. Townsend, Electricity in Gases, Clarendon Press, Oxford, 1915.
[8] A. von Engel, Ionized Gases, Clarendon Press, Oxford, 1955.
[9] Y. Raizer, Gas Discharge Physics, Springer Verlag, Heidelberg, 1991.
[10] M.A. Lieberman, A.J. Lichtenberg, Principles of Plasma Discharges and Materials Processing, John Wiley, New York, 1994.
[11] K.H. Becker, U. Kogelschatz, K.H. Schoenbach, R. Barker (Eds.), Non-Equilibrium Air Plasmas at Atmospheric Pressure. Chapter 9 Applications of Atmospheric-Pressure Air Plasmas, IOP Publ., Bristol, UK, 2004.
[12] E.E. Kunhardt, IEEE Trans. Plasma Sci. 28 (2000) 1.
[13] M.J. Kushner, J. Phys. D 38 (2005) 1633.
[14] K.H. Becker, U. Kogelschatz, K.H. Schoenbach, R.J. Barker (Eds.), Non-equilibrium Air Plasmas at Atmospheric Pressure. Chapter 6, DC and Low-frequency Air Plasma Sources, IOP Publ., Bristol, UK, 2004 (and references therein).
[15] K.H. Schoenbach, R. Verhappen, T. Tessnow, P.F. Peterkin, W. Byszewski, Appl. Phys. Lett. 68 (1996) 13.
[16] P. Kurunczi, H. Shah, K. Becker, J. Phys. B. 32 (1999) L651.

[17] I. Petzenhauser, L.D. Biborosch, U. Ernst, K. Frank, K.H. Schoenbach, Appl. Phys. Lett. 83 (2003) 4297.
[18] D.D. Hsu, D.B. Graves, J. Phys. D 36 (2003) 2898.
[19] H.I. Park, T.I. Lee, K.W. Park, H.K. Baik, Appl. Phys. Lett. 82 (2003) 3191.
[20] Y.-B. Guo, F.C.-N. Hong, Appl. Phys. Lett. 82 (2003) 337.
[21] F. Adler, E. Kindel, E. Davliatchine, J. Phys. D 35 (2002) 2291.
[22] J.W. Frame, D.J. Wheeler, T.A. DeTemple, J.G. Eden, Appl. Phys. Lett. 71 (1997) 1165.
[23] R.M. Sankaran, K.P. Giapis, Appl. Phys. Lett. 79 (2001) 593.
[24] C. Penache, A. Braeuning-Demian, L. Spielberger, H. Schmidt-Boecking, Proceedings of the Hakone VII, vol. 2, Greifswald, Germany, 2000, p. 501.
[25] A.D. White, J. Appl. Phys. 30 (1959) 711.
[26] D.J. Sturges, H.J. Oskam, Appl. Phys. 35 (1964) 2887.
[27] J.W. Gewartkovski, H.A. Watson, Principles of Electron Tubes, Van Nostrand-Reinhold, Princeton, 1965.
[28] K. Becker, K.H. Schoenbach, J.G. Eden, J. Phys. D (in press).
[29] J.W. Frame, J.G. Eden, Electr. Lett. 34 (1998) 1529.
[30] J.G. Eden, S.-J. Park, N.P. Ostrom, S.T. McCain, C.J. Wagner, B.A. Vojak, J. Chen, C. Liu, P. von Allmen, F. Zenhausern, D.J. Sadler, J. Jensen, D.L. Wilcox, J.J. Ewing, J. Phys. D 36 (2003) 2869.
[31] W. Shi, R.H. Stark, K.H. Schoenbach, IEEE Trans. Plasma Sci. 27 (1999) 16.
[32] P. von Allmen, D.J. Sadler, C. Jensen, N.P. Ostrom, S.T. McCain, B.A. Vojak, J.G. Eden, Appl. Phys. Lett. 82 (2003) 4447.
[33] P. von Allmen, S.T. McCain, N.P. Ostrom, B.A. Vojak, J.G. Eden, F. Zenhausern, C. Jensen, M. Oliver, Appl. Phys. Lett. 82 (2003) 2562.
[34] E.E. Kunhardt, K. Becker, US Patent No. 5872426, and subsequent Patent Nos. 6005349, 6147452, 6879103, and 6900592 (1999).
[35] S. Okazaki, M. Kogoma, M. Uehara, Y. Kimura, J. Phys. D 26 (1993) 889.
[36] E.E. Kunhardt, K. Becker, L.E. Amorer, Proceedings of the 12th International Conference on Gas Discharges and their Applications, Greifswald, Germany, 1997, pp. 1–374.
[37] E.E. Kunhardt, K. Becker, L.E. Amorer, L. Palatini, Bull. Am. Phys. Soc. 42 (1997) 1716.
[38] E.E. Kunhardt, G.P. Korfiatis, K. Becker, C. Christodoulatos, in: G.P. Korfiatis (Ed.), Proceedings of the 4th International Conference on Protection and Restoration of the Environment, Halkidiki, Greece, 1998.
[39] N.S. Panikov, A. Paduraru, R. Crowe, P.J. Ricatto, C. Christodoulatos, K. Becker, IEEE Trans. Plasma Sci. 30 (2002) 1424.
[40] L. Moskwinski, P.J. Ricatto, N. Abramzon, K. Becker, G. Korfiatis, C. Christodoulatos, Proceedings of the IV Symposium on Applications of Plasma Processes (SAPP), Jasna, Slovakia, 2003, p. 17.
[41] L.E. Amorer, PhD Thesis, Stevens Institute of Technology, 1999, unpublished.
[42] V. Karanassios, Spectrochim. Acta B 59 (2004) 909.
[43] C. Brede, E. Lundames, T. Greobrokk, S. Pedersen-Bjergaard, J. High Res. Chromatogr. 21 (1998) 633.
[44] U. Engel, A.M. Bilgic, O. Haase, E. Voges, J.A.C. Broekaert, Plasma Sources Sci. Technol. 9 (2000) 1.
[45] A.M. Bilgic, E. Voges, U. Engel, J.A.C. Broekaert, J. Anal. Atom. Spectrom. 15 (2000) 579.
[46] Y. Yin, J. Messier, J.A. Hopwood, IEEE Trans. Plasma Sci. 27 (1999) 1516.
[47] J.A.C. Broekaert, Anal. Bioanal. Chem. 374 (2002) 182.
[48] G. Schaefer, K.H. Schoenbach, in: M. Gundersen, G. Schaefer (Eds.), Physics and Applications of Pseudosparks, Plenum Press, New York, 1990, p. 55.
[49] R.M. Sankaran, K.P. Giapis, J. Appl. Phys. 92 (2002) 2406.
[50] Z.Q. Yu, K. Hoshimiya, J.D. Williams, S.F. Polvinen, G.J. Collins, Appl. Phys. Lett. 83 (2003) 854.
[51] M. Laroussi, Proceedings of the IEEE International Conference on Plasma Science (ICOPS), Monterey, CA, 1999, p. 203;
see also J. Yan, A. el-Dakrouri, M. Laroussi, M. Gupta, J. Vac. Sci. Technol. B20 (2002) 2574.
[52] N. Masoud, K. Martus, K. Becker, Int. J. Mass Spectrom. 233 (2004) 395.
[53] N. Masoud, K. Martus, M. Figus, K. Becker, Contr. Plasma Phys. 45 (2005) 32.
[54] N. Masoud, K. Martus, K. Becker, J. Phys. D 38 (2005) 1674.
[55] R. Foest, E. Kindel, A. Ohl, M. Stieber, K.-D. Weltmann, Plasma Phys. Control. Fusion 47 (2005) B525.
[56] R. Brandenburg, H.-E. Wagner, A.M. Morozov, K.V. Kozlov, J. Phys. D 38 (2005) 1649 (and references therein to earlier publications).
[57] Q. Wang, I. Koleva, V.M. Donnelly, D. Economou, J. Phys. B 38 (2005) 1690.
[58] R.H. Stark, K.H. Schoenbach, J. Appl. Phys. 89 (2001) 3568.
[59] A.P. Yalin, Z.Q. Yu, O. Stan, K. Hoshimiya, A. Rahman, V.K. Surla, G.J. Collins, Appl. Phys. Lett. 83 (2003) 2766.
[60] K. Frank, U. Ernst, I. Petzenhauser, W. Hartmann, Proceedings of Record IEEE International Conference on the Plasma Science, Las Vegas, NV, 2001, p. 381.
[61] M. Moselhy, I. Petzenhauser, K. Frank, K.H. Schoenbach, J. Phys. D: Appl. Phys. 36 (2003) 2922.
[62] E. Badareu, I. Popescu, J. Electr. Contr. 4 (1958) 503.
[63] V.S. Borodin, Yu.M. Kagan, Sov. Phys.: Tech. Phys. 11 (1966) 131.
[64] P. Gill, C.E. Webb, J. Phys. D 10 (1977) 299.
[65] P. Kurunczi, J. Lopez, H. Shah, K. Becker, Int. J. Mass Spectrom. 205 (2001) 277.
[66] S.-M. Yin, C. Christodoulatos, K. Becker, A. Koutsospyros, Proceedings of the International Conference on Environmental System (ICES), SAE International (2003), 2003 (Paper No. 01-2501, on CD ROM).
[67] C. Penache, M. Miclea, A. Braeuning-Demian, O. Hohn, S. Schoessler, T. Jahnke, K. Niemax, H. Schmidt-Boecking, Plasma Sources Sci. Technol. 11 (2003) 476.
[68] R. Block, O. Toedter, K.H. Schoenbach, Proceedings of the 30th AIAA Plasma Dynamics and Lasers Conference, Norfolk, VA, 1999 (Paper No. AIAA-99-3434).
[69] R. Block, M. Laroussi, F. Leipold, K.H. Schoenbach, Proceedings of the 14th International Symposium on Plasma Chemistry, vol. II, Prague, Czech Republic, 1999, p. 945.
[70] P. Kurunczi, N. Abramzon, M. Figus, K. Becker, Acta Phys. Slovaca 54 (2004) 115.
[71] L. Moswinski, PhD thesis, Stevens Institute of Technology, unpublished.
[72] J.P. Boeuf, J. Phys. D: Appl. Phys. 36 (2003) R53.
[73] J.P. Boeuf, L.C. Pitchford, K.H. Schoenbach, Appl. Phys. Lett. 86 (2005) 071501.
[74] B.M. Penetrante, S.E. Schultheiss, Procee of the NATO-ASI, vol. 34A/B, Plenum Press, New York, 1993.
[75] A. Koutsospyros, S.-M. Yin, C. Christodoulatos, K. Becker, Int. J. Mass Spectrom. 233 (2004) 305.
[76] A. Koutsospyros, S.-M. Yin, C. Christodoulatos, K. Becker, IEEE Trans. Plasma Sci. 33 (2005) 42.
[77] K. Becker, A. Koutsospyros, S.-M. Yin, C. Christodoulatos, N. Abramzon, J.C. Joaquin, G. Brelles-Mariño, Plasma Phys. Control. Fusion 47 (2005) B513.
[78] C.M. Nunez, G.H. Ramsey, W.H. Ponder, J.H. Abbott, L.E. Hamel, P.H. Kariher, Air Waste 43 (1993) 242.
[79] B.M. Penetrante, M.C. Hsiao, J.N. Bardsley, B.T. Merrit, G.E. Voglin, A. Kuthiz, C.P. Burkhart, J.R. Bayless, Plasma Sources Sci. Technol. 6 (1997) 251.
[80] S. Futurama, A. Zhang, G. Prieto, T. Yamamoto, IEEE Trans. Ind. Appl. 34 (1998) 967.
[81] M. Laroussi, J.P. Richardson, F.C. Dobbs, Appl. Phys. Lett. 81 (2002) 772.
[82] C.L. Nelson, T.J. Berger, Curr. Microbiol. 18 (1989) 275.
[83] M. Laroussi, IEEE Trans. Plasma Sci. 24 (1996) 1188.
[84] H.W. Hermann, I. Henins, J. Park, G.S. Salwyn, Phys. Plasmas 6 (1999) 2284.
[85] M. Laroussi, I. Alexeff, W.L. Kang, IEEE Trans. Plasma Sci. 28 (2000) 184.

[86] D.A. Mendis, M. Rosenberg, F. Azam, IEEE Trans. Plasma Sci. 28 (2000) 1304.
[87] N.M. Efremov, B.Y. Adamiak, V.I. Blochin, S.J. Dadashev, K.I. Dimitiev, O. Gryaznova, V.F. Jubashev, IEEE Trans. Plasma Sci. 28 (2000) 238.
[88] J.G. Birmingham, D.J. Hammerstrom, IEEE Trans. Plasma Sci. 28 (2000) 51.
[89] T.C. Montie, K. Kelly-Wintenberg, J.R. Roth, IEEE Trans. Plasma Sci. 28 (2000) 41.
[90] S. Lerouge, M.R. Werthheimer, R. Marchand, M. Tabrizian, L.H. Yahia, J. Biomed. Mater. Res. 51 (2000) 128.
[91] S. Moreau, M. Moisan, J. Barbeau, J. Pelletier, A. Ricard, J. Appl. Phys. 88 (2000) 1166.
[92] M. Moisan, J. Barbeau, S. Moreau, J. Pelletier, M. Tabrizian, L.H. Yahia, Int. J. Pharm. 226 (2001) 1.
[93] M. Laroussi, IEEE Trans. Plasma Sci. 30 (2002) 1409.
[94] M. Laroussi, A. Mendis, M. Rosenberg, New J. Phys. 5 (2003) 41.1.
[95] M. Laroussi, in: K.H. Becker, U. Kogelschatz, K.H. Schoenbach, R.J. Barker (Eds.), Biological Decontamination Using Non-equilibrium Atmospheric Air Plasmas, Section 9.9, IOP Publ., Bristol, UK, 2004 (and references therein).
[96] M. Laroussi, F. Leipold, Int. J. Mass Spectrom. 233 (2004) 81.
[97] J.C. Joaquin, N. Abramzon, and G Brelles-Mariño, Appl. Environ. Microbiol. (submitted for publication).
[98] P. Kurunczi, K. Martus, K. Becker, Int. J. Mass. Spectrom. 223–224 (2003) 37.
[99] K.H. Schoenbach, A. El-Habachi, M. Moselhy, W. Shi, R.H. Stark, Phys. Plasmas 7 (2000) 2186.
[100] M. Moselhy, K.H. Schoenbach, J. Appl. Phys. (2004).
[101] A. El-Habachi, K.H. Schoenbach, Appl. Phys. Lett. 72 (1998) 22.
[102] A. El-Habachi, K.H. Schoenbach, Appl. Phys. Lett. 73 (1998) 885.
[103] K.H. Schoenbach, M. Moselhy, W. Shi, R. Bentley, J. Vac. Sci. Technol. A 21 (2003) 1260.
[104] A. El-Habachi, W. Shi, M. Moselhy, R.H. Stark, K.H. Schoenbach, J. Appl. Phys. 88 (2000) 3220.
[105] M. Moselhy, R.H. Stark, K.H. Schoenbach, U. Kogelschatz, Appl. Phys. Lett. 78 (2001) 880.
[106] K. Martus, N. Masoud, and K. Becker, Plasma Sources Sci. Technol. (in press).
[107] J.J. Thomson, Rays of Positive Electricity and Their Application to Chemical Analyses, Longmans, Green, 1913.
[108] M. Miclea, K. Kunze, U. Heitmann, J. Franzke, K. Niemax, J. Anal. Atom. Spectrom. 19 (2004) 990.
[109] M. Miclea, K. Kunze, U. Heitmann, S. Florek, J. Franzke, K. Niemax, J. Phys. D 38 (2005) 1709.
[110] C. Jost, D. Sprung, T. Kenntner, T. Reiner, Int. J. Mass Spectrom. 223–224 (2003) 771.
[111] S. Peng, N. Ahlmann, K. Kunze, W. Nigge, M. Edler, T. Hoffmann, J. Franzke, Rapid Commun. Mass Spectrom. 18 (2004) 1803.
[112] J.C.T. Eijkel, H. Stoeri, A. Manz, Anal. Chem. 71 (1999) 2600.
[113] J.C.T. Eijkel, H. Stoeri, A. Manz, Anal. Chem. 72 (2000) 2547.
[114] M. Miclea, K. Kunze, U. Heitmann, G. Musa, J. Franzke, K. Niemax, Spectrochim. Acta B 56 (2001) 37.
[115] M. Miclea, K. Kunze, J. Franzke, K. Niemax, Spectrochim. Acta B 57 (2002) 1585.
[116] K. Kunze, M. Miclea, J. Franzke, K. Niemax, Spectrochim. Acta B 58 (2003) 1435.
[117] A. Bass, C. Chevalier, M.W. Blades, J. Anal. Atom. Spectrom. 16 (2001) 919.
[118] R. Guchardi, P.C. Hauser, J. Anal. Atom. Spectrom. 19 (2004) 945.
[119] X. Quan, S. Chen, B. Platzer, J. Chen, M. Gfrerer, Spectrochim. Acta B 57 (2002) 189.
[120] C. Brede, S. Pedersen-Bjergaard, E. Lundanes, T. Greibrokk, Anal. Chem. 70 (1998) 513.
[121] O.B. Minayeva, J.A. Hopwood, J. Anal. Atom. Spectrom. 18 (2003) 856.
[122] A.M. Bilgic, U. Engel, E. Voges, M. Kückelheim, J.A.C. Broekaert, Plasma Sources Sci. Technol. 9 (2000) 1.
[123] A.M. Bilgic, E. Voges, U. Engel, J.A.C. Broekaert, J. Anal. Atom. Spectrom. 15 (2000) 579.
[124] U. Engel, A.M. Bilgic, O. Haase, E. Voges, J.A.C. Broekaert, Anal. Chem. 72 (2000) 193.
[125] P. Siebert, G. Petzold, A. Hellenbart, J. Müller, Appl. Phys. A 67 (1998) 155.
[126] T. Ichiki, R. Taura, Y. Horiike, J. Appl. Phys. 95 (2004) 35.
[127] R.E.J. Sladek, E. Stoffels, R. Walraven, P.J.A. Tielbeck, R.A. Koolhoven, IEEE Trans. Plasma Sci. 32 (2004) 1540.
[128] R. Rahul, O. Stan, A. Rahman, E. Littlefield, K. Hoshimiya, A.P. Yalin, A. Sharma, A. Pruden, C.A. Moore, Z. Yu, G.J. Collins, J. Phys. D: Appl. Phys. 38 (2005) 1750.
[129] A. Ignatkov, A. Schwabedissen, G.F. Leu, J. Engemann, Contr. Papers, Hakone VIII (Pühajärve, Estonia) 1 (2002) 58.